Method for Diagnosing a Short-Circuit Fault in the Stator Winding of a Motor Based on Parameter Identification of Features and a Support Vector Machine

Hisahide Nakamura [1,*] and Yukio Mizuno [2,*]

[1] Research and Development Division, TOENEC Corporation, 1-79, Takiharu-cho, Minami-ku, Nagoya 457-0819, Japan

[2] Department of Electrical and Mechanical Engineering, Nagoya Institute of Technology, Gokiso-cho, Showa-ku, Nagoya 466-8555, Japan

* Correspondence: hisahide-nakamura@toenec.co.jp (H.N.); mizuno.yukio@nitech.ac.jp (Y.M.); Tel.: +81-52-619-1707 (H.N.); +81-52-735-5439 (Y.M.)

Abstract: Motors are widely used in various industrial fields as key power sources, and their importance is increasing. According to the failure occurrence rates of the parts in an electric motor, a short-circuit fault of the winding due to the deterioration of the insulation is among the most probable. An easy and effective method for diagnosing faults is needed to ensure the working condition of a motor with high reliability. This paper proposes a novel method for diagnosing a slight turn-to-turn short-circuit fault in a stator winding that involves an impulse test, parameter identification, and diagnosis. In this work, impulse tests were conducted; the measured voltage characteristics are discussed. Next, the parameter identification of the coefficients of the equivalent circuit of the impulse test was performed using particle swarm optimization. Finally, diagnosis was performed based on a support vector machine that has high classification ability, and the effectiveness of the proposed method was verified experimentally.

1. Introduction

Currently, motors are used widely in various industrial fields as key power sources, and their importance is increasing. According to the failure occurrence rates of the parts in a motor, the stator winding is among those most likely to fail, accounting for up to 25% of all failures [1,2].

Typically, a stator fault is due to the breakdown of the insulation between turns, and it has been reported that approximately 80% of all electrical failures in the stator are due to the failure of the winding insulation [3], which, in turn, is due to a combination of mechanical, electrical, thermal, and environmental stresses.

If a stator winding suffers a short-circuit fault (SCF), it can rapidly develop into a more serious fault, such as ground fault or even a fire. Therefore, SCFs are among the most critical faults that must be detected. If an SCF is detected early under relatively minor conditions, then an effective remedy can be taken to avert disaster. Accordingly, an easy and effective method for fault diagnosis is needed to ensure the operating condition of a motor with high reliability.

If an SCF occurs, it could cause significant damage to the stator core. A stator-core quality assessment technique has been reported for evaluating the condition of a stator core [4]. Fortunately,

there has been sufficient research on the detection and diagnosis of SCFs, and many methods have been proposed over the past two decades [5–8]. Among these methods, the impulse test is the only test that can find a minor SCF [9]. Though this test is performed off-line, it is useful for finding faults and assessing the condition of a coil. The impulse test is widely used on site and is still being improved [10–12].

In the impulse test, an impulse voltage is applied between the terminals, and the voltage between the windings is measured. The diagnostic method based on the impulse test focuses on the shape of the voltage waveform. Because this shape differs between a healthy winding and one with an SCF, a judgment is made by calculating the area over which two waveforms are out of position. However, the area itself has no physical meaning and cannot be used to diagnose the fault mode (e.g., a one-turn or two-turn SCF).

This paper proposes a novel method for the detailed diagnosis of a slight turn-to-turn SCF in a stator winding. First, an impulse generator that generates a relatively low impulse voltage is developed. This impulse generator is used to conduct an impulse test, and the voltage characteristics are discussed. Subsequently, the coefficients of the equivalent circuit of the impulse test are identified, and particle swarm optimization (PSO) is used to solve the optimization problem to find the optimal solution for the coefficients. Finally, diagnosis is performed based on a support vector machine (SVM) that has high classification ability, and the effectiveness of the proposed method is verified experimentally.

2. Impulse Test

2.1. Equivalent Circuit

In the impulse test (also known as the surge test), an impulse voltage is applied across the target winding of the motor. In this section, impulse tests are carried out, the voltages between terminals are measured, and the characteristics are discussed.

The experimental setup of the impulse test is shown in Figure 1. The impulse generator comprises a DC power source, a capacitor charged by the power source, and a switch. When the switch is moved to the ON position, the impulse voltage is generated by the capacitor and quickly discharges into the winding. During the discharge, the resistance and inductance of the stator winding form a series circuit.

Since the stator winding configures a star-connection, the motor has three terminals: U, V, and W. An impulse voltage is applied between terminals U and V, V and W, or W and U. Figure 1 shows a circuit connection when an impulse voltage is applied between terminals U and V (denoted as U–V).
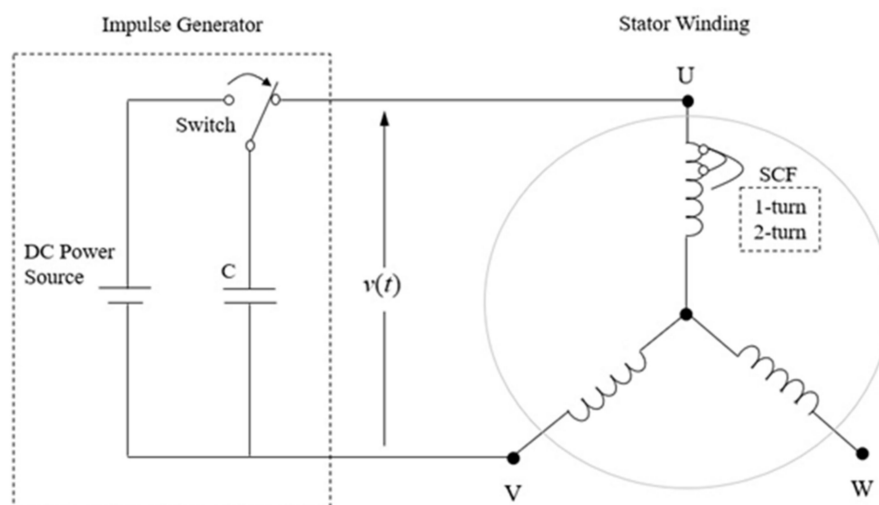
Figure 1. Experimental setup of impulse test.

2.2. Measurement of Voltage

The impulse generator is shown in Figure 2. It can generate a voltage of up to 40 V for application to the terminals. To ensure that the capacitor discharges quickly, a field-effect transistor is used as the switch. The generator contains an analog-to-digital converter; the analog signal of the measured voltage is converted to a digital signal that is then transferred to an external PC via a USB cable and stored on the hard disk of the PC. The sampling time can be varied from 1 to 100 μsec but was fixed at 10 μsec in this experiment.
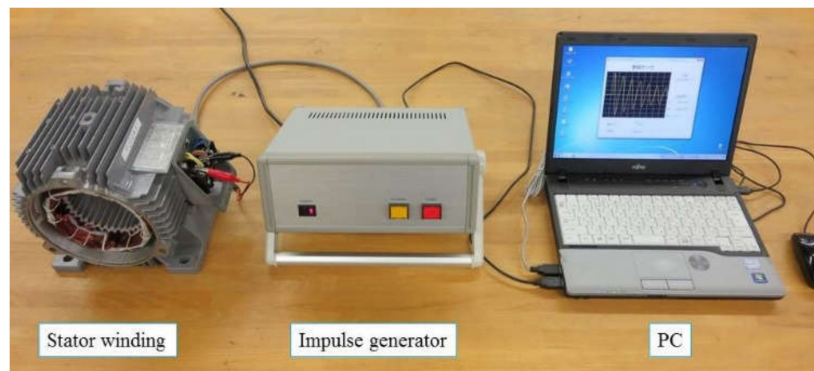
Figure 2. Developed impulse generator.

2.3. Reproduction of Short-Circuit Fault

The stator winding of an induction motor (1.5 kW, 200 V, 6.2 A, four poles) was used as a specimen. This stator winding has double star connection and 92 turns per phase. This motor was tentatively named motor 1. To confirm the voltage characteristic, a stator winding with SCFs was needed. However, collecting a sufficient number of such windings from actually damaged motors would have taken a long time and been expensive. Therefore, artificially induced SCFs were used in the present study. The SCFs were made by removing the enamel insulation at two points in the winding and connecting them with solder, as shown in Figure 3. Herein, the connection between the first and second turns of the stator winding is referred to as the one-turn SCF.
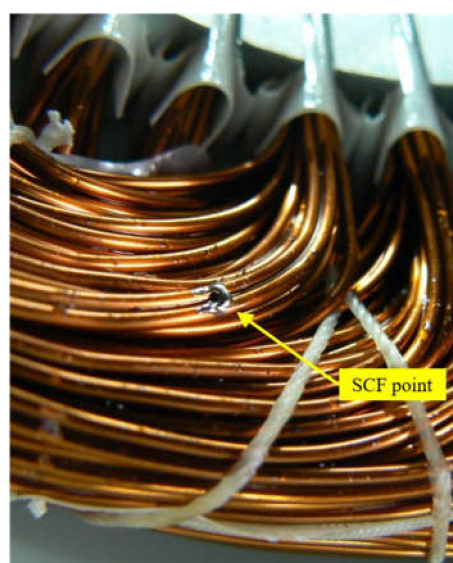
Figure 3. Reproduction of a short-circuit fault (SCF).

2.4. Voltage Characteristics in Impulse Test

Impulse tests were implemented between the terminals of a healthy, one-turn SCF and two-turn SCF stator windings. These results are shown in Figures 4–6, respectively. In these figures, the green, the blue, and the red lines correspond to the voltage waveform between the terminals of U–V, V–W, and W–U, respectively. From Figure 4, it is clear that the three voltage waveforms measured between the terminals of the healthy winding had almost the same shape.
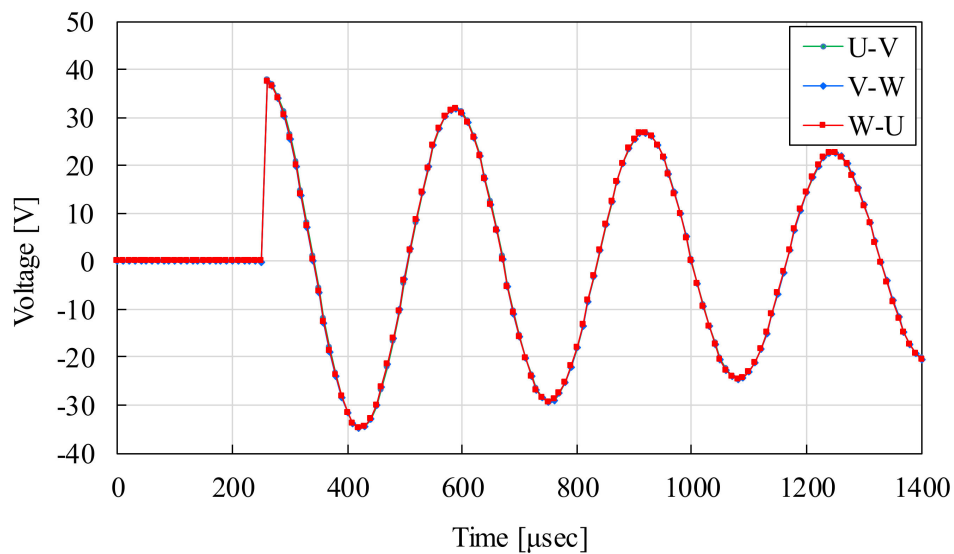
Figure 4. Waveform of a healthy winding.
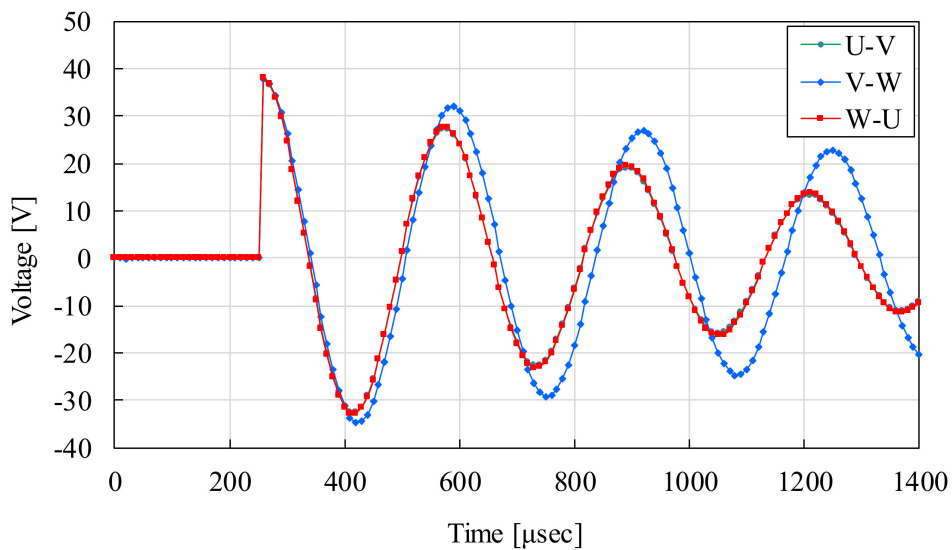
Figure 5. Waveform of a one-turn SCF.
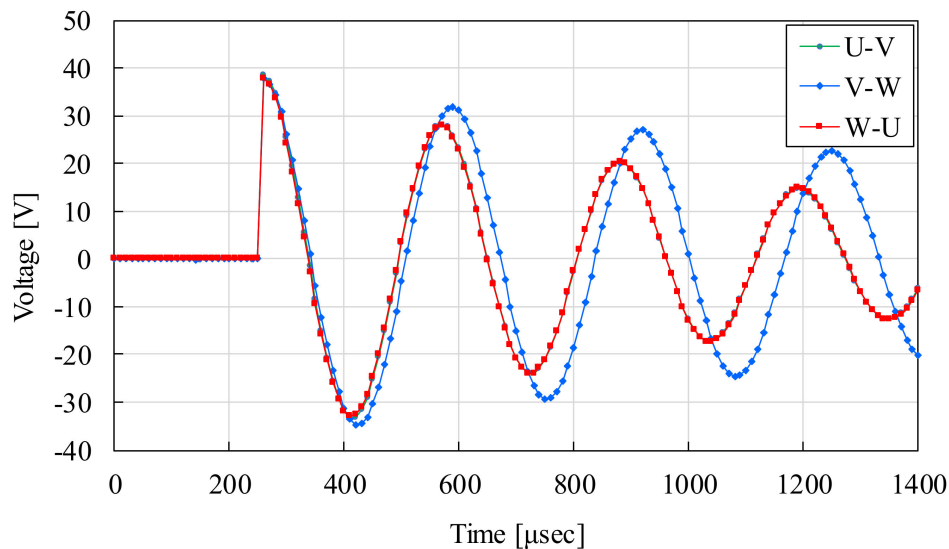
Figure 6. Waveform of a two-turn SCF.

Next, when a one-turn or two-turn SCF occurred in the U phase winding, the shapes of the voltage waveforms of U–V and W–U, including the U phase, significantly changed compared with that of the healthy winding of V–W. This was due to the change of resistance and the inductance of the U phase winding. By contrast, the U–V and W–U waveforms were almost the same.

For comparison of voltage waveforms under different winding conditions, waveforms across the U–V terminals shown in Figures 4–6 were merged and are demonstrated in Figure 7. From Figure 7, we can see that the frequency of the vibration got higher as the number of short-circuit turn increased.
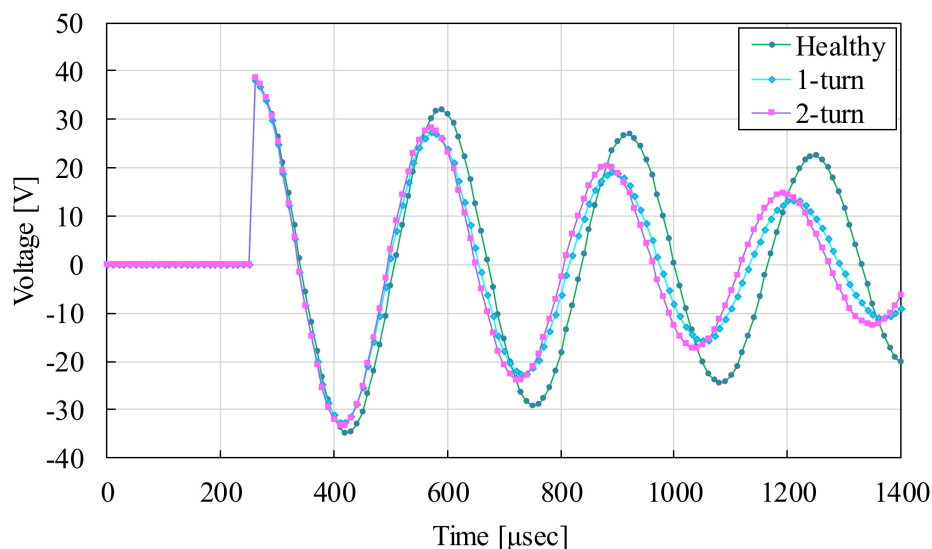
Figure 7. Voltage waveforms across U–V terminals obtained for healthy, one-turn SCF, and two-turn SCF windings.

In this impulse test, under the same winding conditions, the impulse voltage was applied repeatedly 15 times for the healthy and faulty windings. As a result, it was confirmed that the 15 waveform shapes were almost the same under the same winding conditions. The similarity of the waveforms was evaluated by the correlation coefficient, which represented the degree of similarity and took a value between 1 and −1. As the value of the coefficient approached 1, there was a strong

correlation between two waveforms. In this evaluation, 15 waveforms obtained from the healthy winding of U–V were used, and the correlation coefficients between the first waveform and each waveform of the remaining 14 waveforms were calculated. The average value was 0.9998. Furthermore, the maximum value and minimum value of the coefficient were 0.9999 and 0.9995, respectively. This means that there was a high similarity between the waveforms. Likewise, average correlation coefficients of 0.9998 and 0.9981 were obtained in the case of the one- and two-turn SCFs in the winding, respectively. From these results, the shapes of the voltage waveforms measured in the impulse test depended on the winding condition, and it is evident that their waveforms had a strong similarity and highly reproducibility under the same winding condition.

3. Parameter Identification

3.1. Feature Extraction

As the first step in diagnosis, the effective features must be extracted, and in this section, the manner in which this is achieved is presented. The experimental setup of the impulse test shown in Figure 1 is considered. Based on the circuit, suppose that the voltage across the winding is $v(t)$, the resistance of the circuit is R, the inductance is L, and the capacitance is C. In this circuit, the resistance and the inductance components of the winding account for a large percentage in R and L, respectively. Then, the following equation is obtained:

$$LC\frac{d^2v(t)}{dt^2} + RC\frac{dv(t)}{dt} + v(t) = 0 \tag{1}$$

By transforming Equation (1) into a difference equation, the following equation can be obtained:

$$LC\frac{v[n+2] - 2v[n+1] + v[n]}{T_s^2} + RC\frac{v[n+2] - v[n]}{2T_s} + v[n+1] = 0 \tag{2}$$

where T_s is the sampling time. Furthermore, by rearranging Equation (2), the following equation is obtained:

$$v[n+2] = a_1 v[n+1] + a_2 v[n] \quad (n = 0, 1, 2, \cdots) \tag{3}$$

where

$$a_1 = \left(\frac{2LC}{T_s^2} - 1\right) \bigg/ \left(\frac{LC}{T_s^2} + \frac{RC}{2T_s}\right) \tag{4}$$

$$a_2 = \left(-\frac{LC}{T_s^2} + \frac{RC}{2T_s}\right) \bigg/ \left(\frac{LC}{T_s^2} + \frac{RC}{2T_s}\right) \tag{5}$$

In this study, both LC and RC, which are included in the coefficients a_1 and a_2, are regarded as features whereupon parameter identification is performed.

3.2. Parameter Identification Based on PSO

According to Equation (3), the features of LC and RC are included in both the numerator and denominator in each a_1 and a_2. It is impossible to derive LC and RC analytically, so they must instead be calculated numerically. For this reason, PSO was used for the parameter identification of (LC, RC) in this study. Further, a brief description of PSO is provided. PSO was originally proposed to simulate the flocking behavior of birds and fish [13]. Because the advantages of PSO are that (i) its algorithm is simple and easy to understand and (ii) it is easy to implement, it is used widely as a tool to solve optimization problems, and several applications for it have been proposed [14–17].

The basic idea of the algorithm is to update both the velocity and position of the particles using the following equations:

$$v_i(t+1) = w \times v_i(t) + c_1 \times rand() \times \left(p_i^{best} - p_i(t)\right) + c_2 \times rand() \times \left(p_{gbest} - p_i(t)\right) \tag{6}$$

$$p_i(t+1) = p_i(t) + v_i(t+1) \tag{7}$$

where w is an inertial weight; c_1 and c_2 are acceleration coefficients; $rand()$ is a random value between 0 and 1; $v_i(t)$ and $p_i(t)$ are the velocity and position, respectively, of the ith particle at time t; p_i^{best} is the best position of the ith particle; and p_{gbest} is the swarm's best position as of time t.

PSO is used to find the optimal (LC, RC) that minimize e described by the following equation:

$$e = \sum_{n=0}^{N} (v[n+2] - (a_1 v[n+1] + a_2 v[n]))^2 \tag{8}$$

To identify LC and RC, 40 points of $v(t)$ that correspond to one or more cycles of the waveform are used. The parameters used in PSO are given in Table 1.

Table 1. Parameters of particle swam optimization (PSO).

Item	Value
Number of Particles	100
Interactions	100
w	0.1
C_1	0.1
C_2	0.1

The calculation process of PSO is shown in Figure 8; 100 particles are used in this calculation. Initially, they are arranged in a grid in the solution space (Figure 8a). Then, they are moved following Equations (6) and (7). As the number of iterations increases, 100 particles converge to a point. After 40 iterations, 100 particles are almost converged at one point (Figure 8f). In this parameter identification, the best particle that minimizes above-mentioned e is selected as (LC, RC).

(a)

(b)

Figure 8. *Cont.*

(c)

(d)

(e)

(f)
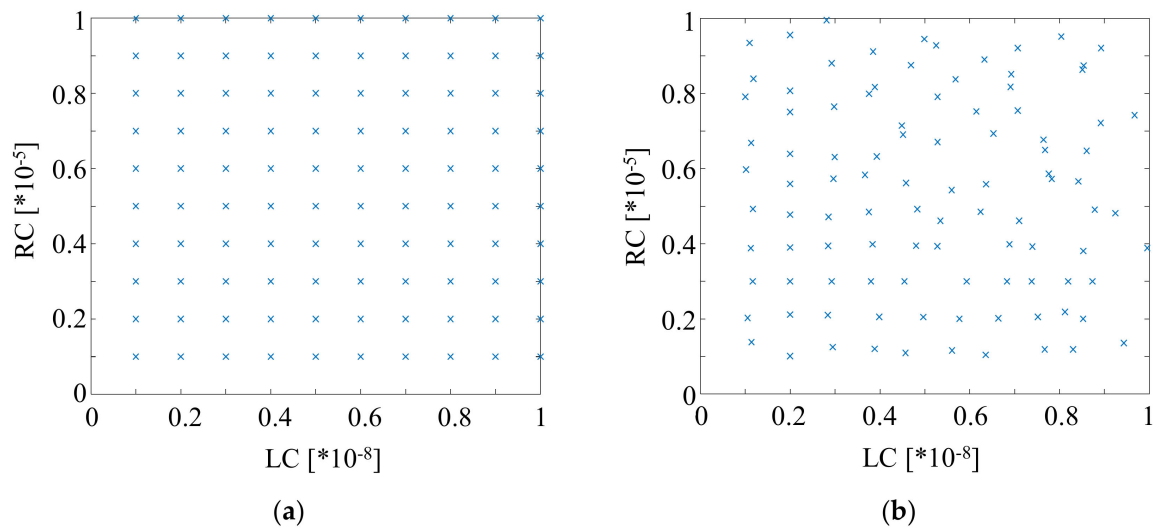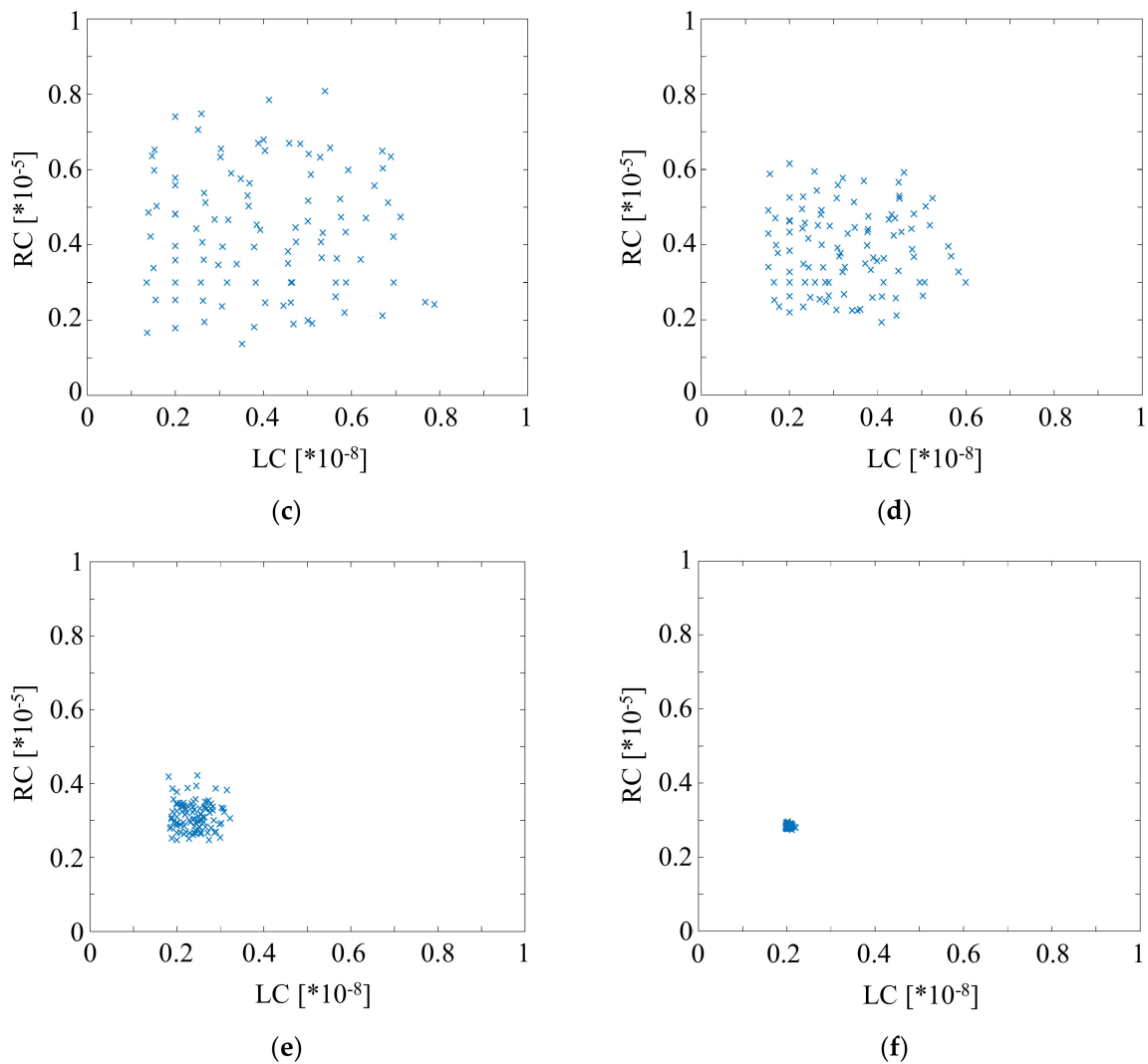
Figure 8. Calculation process of PSO. (**a**) Iteration is 0; (**b**) iteration is 1; (**c**) iteration is 5; (**d**) iteration is 10; (**e**) iteration is 20; and (**f**) iteration 40.

4. Feature Distribution Analysis

Parameter identification based on PSO was carried out for the voltage waveforms obtained in the impulse tests. In this parameter identification, the impulse tests were repeated five times, and the waveforms obtained from U–V under each winding condition were used. The feature distributions of *LC* and *RC* obtained by PSO are shown in Figure 9. Thus, it can be clarified that the areas in which *LC* and *RC* are distributed were different and were distributed in almost the same area based on the winding conditions.
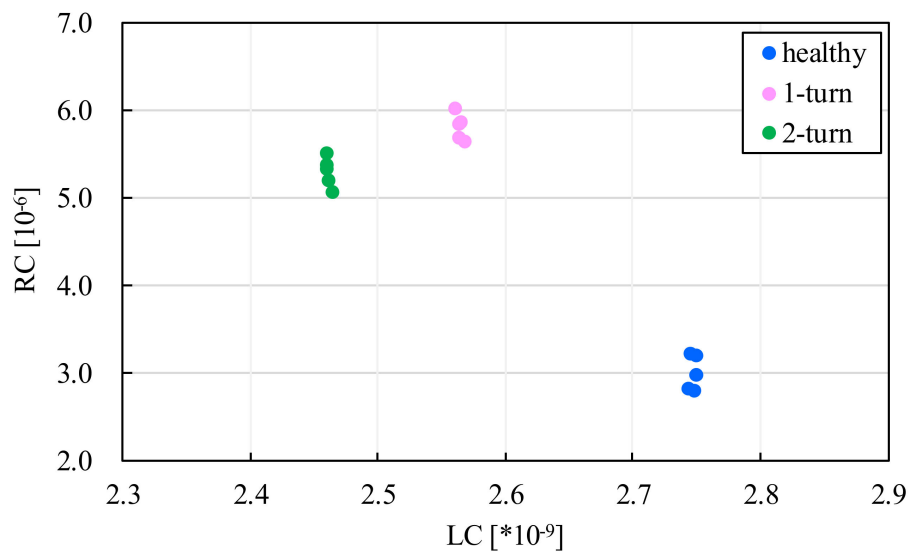
Figure 9. Feature distribution for the 1.5-kW motor 1.

Next, as a consistency test, a new motor, named motor 2, was prepared; it was of the same type as motor 1 but was from a different production lot, and the impulse test was performed again. The identified result for *LC* and *RC* of the new motor is shown in Figure 10. As can be seen by comparing Figures 9 and 10, the features were again distributed in the same area according to the winding conditions. A high similarity and repeatability of voltage waveforms at a given winding condition were also confirmed by the same procedures described in Section 2.4. In a careful manner, evaluation was carried out using two more motors, and consistency was demonstrated.
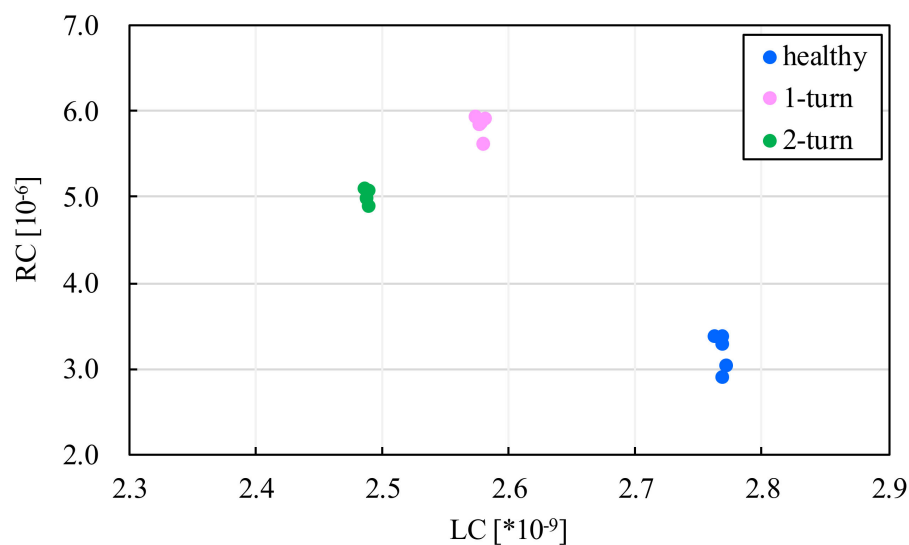
Figure 10. Feature distribution for the 1.5-kW motor 2.

For evaluation using another type of motor, a new 2.2-kW motor, namely motor 1, was prepared with a winding whose constitution differed from that of the 1.5-kW motor. One-turn and two-turn SCFs were introduced in the W phase of this motor, and five repeated impulse tests were carried out. By using the waveforms obtained from V–W, *LC* and *RC* were identified. The result is shown in Figure 11, from which it can be seen that the values of *LC* and *RC* tended to be distributed in the same area depending on the winding conditions, as with the result for the 1.5-kW motor.
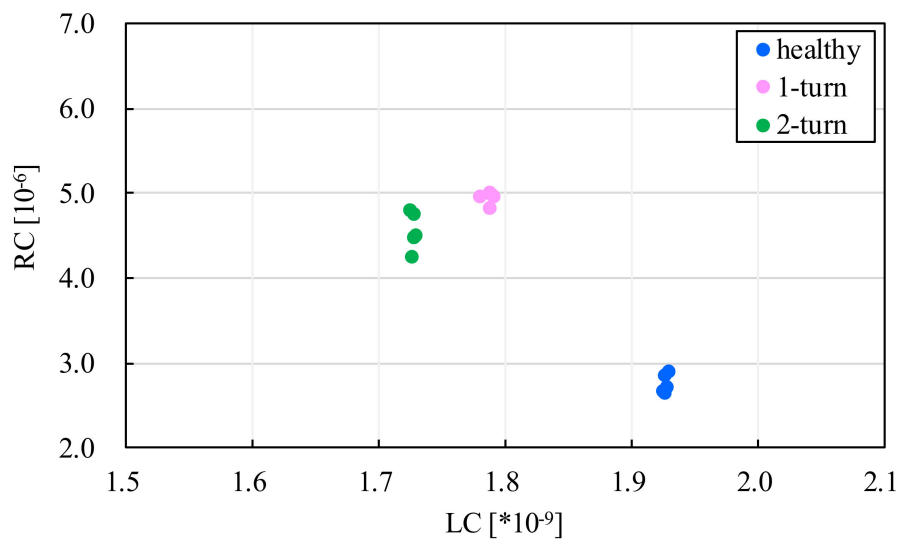
Figure 11. Feature distribution for the 2.2-kW motor 1.

Considering all results described above, *LC* and *RC* reflect the winding condition very well and were highly reliable features to judge a slight turn-to-turn SCF of the winding.

We considered the physical meaning of *LC*. A resonance angular frequency ω of the serial circuit shown in Figure 1 is represented as $\omega = 1/\sqrt{LC}$. The resonance frequency is as follows: $f = \omega/2\pi$. This means that *LC* represents the degree of change in a time axis direction. The resonance frequencies under the healthy, one-turn SCF and two-turn SCF conditions shown in Figures 4–6 were 3.05, 3.15, and 3.20 kHz, respectively. On the other hand, the resonance frequencies induced by *LC*, which were calculated by PSO, were 3.04, 3.14, and 3.21 kHz, respectively. Those were almost the same. The resonance frequency was easily induced from the parameter *LC*.

Thus, instead of using only one feature (that of the area value between healthy and faulty waveforms), using two features (*LC* and *RC*) can provide more useful information for diagnosis.

5. Diagnosis of Stator Windings

5.1. Support Vector Machine

The diagnostic tool used in this study was an SVM, which is a supervised machine-learning algorithm [18]. The SVM concept is based on the margin, which is defined as the distance between the decision boundary and the closest of the data points. The SVM maximizes this margin to find the decision boundary, called the hyperplane, which produces optimal separation of classes. SVMs were originally introduced to classify linear classes. However, as well as performing linear classification, they can efficiently perform nonlinear classification using a kernel. Because the advantages of SVMs are their high discrimination ability and easy implementation for nonlinear discrimination, they are widely used for classification problems and other applications [19–21].

There are two types of SVM, namely a hard-margin SVM and a soft-margin SVM. A hard-margin SVM offers a very low degree of misrecognition, whereas a soft-margin SVM allows for some degree of misrecognition. In the present study, a soft-margin SVM was used; this SVM has two important parameters, namely cost and γ parameters. A smaller value of the cost parameter allows for misrecognition, while a larger value of the cost parameter allows for no misrecognition and the SVM behaves as a hard-margin SVM. Meanwhile, the larger the value of γ parameter, the more complex the boundary.

5.2. Diagnosis for 1.5-kW Motor

First, the 1.5-kW motor described in Section 2 was diagnosed. Five combinations of *LC* and *RC* obtained from U–V of motor 1 under each winding condition were used as the training data, and 10 combinations of *LC* and *RC* obtained from motor 2 were used as the verification data. A motor of the same type, namely motor 3, was also prepared, and 10 combinations of *LC* and *RC* were calculated and were used as verification data.

The SVM-based diagnosis was implemented in the free software *R*, which is a programming language that is used widely for statistical computing. The values of cost and γ parameters used in the SVM are given in Table 2. In general, they need to be chosen optimally. The software *R* automatically chooses their certain optimal values.

Table 2. Parameters of the support vector machine (SVM).

Item	Value
Type of SVM	Soft Margin SVM
Kernel	Radial
Cost Parameter	1
γ Parameter	0.5

The diagnostic results for motors 2 and 3 are given in Tables 3–6. These results showed that for all three winding conditions, the proposed method correctly diagnosed not only the difference between a healthy winding and a faulty one but also the difference between a one-turn SCF and a two-turn SCF.

Table 3. Diagnostic results for the 1.5-kW motor 2 (healthy).

	Winding Condition	U–V	V–W	W–U
Results of Diagnosis	Healthy	10	10	10
	One-Turn Short-Circuit	0	0	0
	Two-Turn Short-Circuit	0	0	0

Table 4. Diagnostic results for the 1.5-kW motor 2 (one-turn short-circuit in the U phase winding).

	Winding Condition	U–V	V–W	W–U
Results of Diagnosis	Healthy	0	10	0
	One-Turn Short-Circuit	10	0	10
	Two-Turn Short-Circuit	0	0	0

Table 5. Diagnostic results for the 1.5-kW motor 2 (two-turn short-circuit in the U phase winding).

	Winding Condition	U–V	V–W	W–U
Results of Diagnosis	Healthy	0	10	0
	One-Turn Short-Circuit	0	0	0
	Two-Turn Short-Circuit	10	0	10

Table 6. Diagnostic results for the 1.5-kW motor 3 (healthy).

	Winding Condition	U–V	V–W	W–U
Results of Diagnosis	Healthy	10	10	10
	One-Turn Short-Circuit	0	0	0
	Two-Turn Short-Circuit	0	0	0

5.3. Diagnosis for 2.2-kW Motor

Next, the 2.2-kW motor was diagnosed. As with the 1.5-kW motor, five combinations of *LC* and *RC* obtained from V–W of motor 1 under each winding condition were used as the training data, and 10 combinations of *LC* and *RC* obtained from motor 2 were used as the verification data. The U phase of motor 2 contained a two-turn SCF.

In this diagnosis, a motor of the same type, namely motor 3, was also prepared, and 10 combinations of *LC* and *RC* were calculated under healthy conditions and were used as verification data.

The diagnostic results for motors 2 and 3 are presented in Tables 7–9. As shown in Table 8, the two-turn SCF was incorrectly judged as being a one-turn SCF only once, but the remaining results were recognized correctly. At the very least, the difference between a healthy winding and a faulty winding could be determined correctly. The global accuracy was 99.5% (209/210). The above results showed that the proposed method enables extremely accurate diagnosis, and no problems are expected in its practical use.

Table 7. Diagnostic results for the 2.2-kW motor 2 (healthy).

	Winding Condition	**U–V**	**V–W**	**W–U**
Results of Diagnosis	Healthy	10	10	10
	One-Turn Short-Circuit	0	0	0
	Two-Turn Short-Circuit	0	0	0

Table 8. Diagnostic results for the 2.2-kW motor 2 (two-turn short-circuit in the U phase winding).

	Winding Condition	**U–V**	**V–W**	**W–U**
Results of Diagnosis	Healthy	0	10	0
	One-Turn Short-Circuit	0	0	1
	Two-Turn Short-Circuit	10	0	9

Table 9. Diagnostic results for the 2.2-kW motor 3 (healthy).

	Winding Condition	**U–V**	**V–W**	**W–U**
Results of Diagnosis	Healthy	10	10	10
	One-Turn Short-Circuit	0	0	0
	Two-Turn Short-Circuit	0	0	0

5.4. Discussion for Practical Use

As the number of PSO iterations increased, *LC* and *RC* converged to a certain value, but this required a not insignificant calculation time. To apply this method on site, the number of PSO iterations must be determined by taking into account both the convergence and the calculation time. Because a random function is used in the PSO algorithm, as shown in Equation (6), the solutions differed slightly even when the same data were used. Parameter identification was performed 10 times for one set of data while changing the number of iterations, and the relationship between the number of iterations and the calculated optimum solution of *LC* was evaluated. The results are shown in Figure 12, according to which *LC* had yet to converge after 10 iterations. However, the convergence of *LC* improved as the number of iterations increased, and *LC* approached convergence after 40 iterations. From this result, there should be at least 40 iterations.
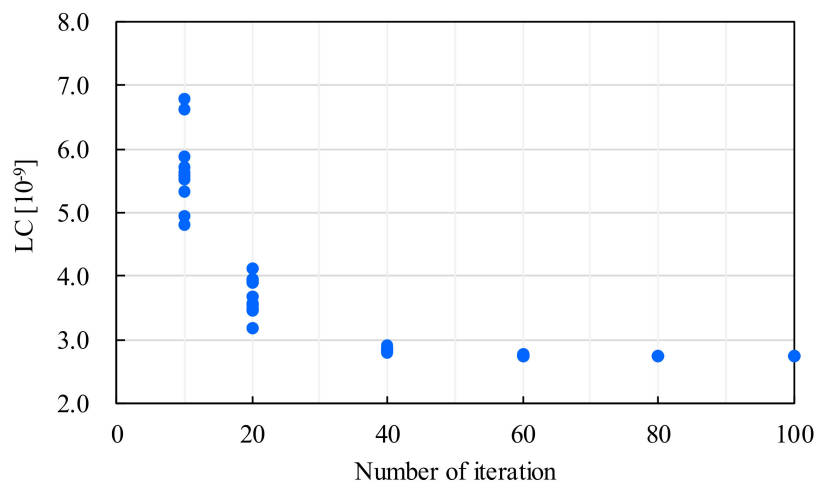
Figure 12. Relationship between number of iterations and value of *LC* (a feature whereupon parameter identification was performed).

Regarding the calculation time, when a 32-bit computer (Core i5, 3.2 GHz) was used for this calculation, it took approximately 10 s until *LC* and *RC* had converged after 40 iterations. Though the convergence time depends on parameters such as w, c_1, and c_2 in the PSO algorithm, the selection of optimum values of these parameters has yet to be examined, and optimum programing has yet to be considered. It follows from this that calculation time could be reduced by selecting optimum values and applying optimum programing. Another measure that could reduce the calculation time is narrowing the search space of *LC* and *RC*. However, studying how to reduce the calculation time is left for future work.

6. Conclusions

This study proposed a novel method—involving an impulse test, parameter identification, and diagnosis—to diagnose slight turn-to-turn SCFs in motor windings. First, impulse tests were carried out, and the voltage characteristics were discussed. The results showed that for the winding of a motor of several kilowatts, the voltage waveforms differed largely between healthy and faulty conditions, even if a low impulse voltage was used instead of a high one of the order of several kilovolts. Specifically, the advantages of using a low impulse voltage instead of a high one are that (i) there is no risk of breaking the insulation of the winding and (ii) the impulse generator can be made smaller. Next, PSO was used to perform parameter identification for features induced by the equivalent circuit of the impulse test.

By representing the difference between healthy and SCF conditions, *LC* and *RC* could be explicitly displayed in the two-dimensional distribution of *LC* and *RC*. We could visually and easily identify the conditions of the windings by the region where *LC* and *RC* existed.

Finally, diagnosis was performed using an SVM. The results showed that even the difference between a one-turn SCF and a two-turn SCF was diagnosed mostly accurately, and the effectiveness of the proposed method was verified.

The resonance frequency of the equivalent circuit of the impulse test is easily induced from the parameter *LC*. This can be used as an effective index value of the product management of the stator winding.

The application of the proposed method to an incipient fault or pre-short-circuit fault with resistance is a challenging work. The authors would like to try it in the future.

Conflicts of Interest: The authors declare no conflict of interest.

References

1. Nandi, S.; Toliyat, H.; Li, X. Condition Monitoring and Fault Diagnosis of Electrical Motors—A Review. *IEEE Trans. Energy Convers.* **2005**, *20*, 719–729. [CrossRef]
2. IAS Motor Reliability Working Group. Report of Large Motor Reliability Survey of Industrial and Commercial Installations. *IEEE Trans. Ind. Appl.* Part I. **1985**, *IA-21*, 865–872. [CrossRef]
3. Geiman, J. *DC Step-Voltage and Surge Testing Motors*; Baker Instrum. Co.: Fort Collins, CO, USA, 2007.
4. Lee, K.; Hong, J.; Lee, K.-W.; Bin Lee, S.; Wiedenbrug, E. A Stator-Core Quality-Assessment Technique for Inverter-Fed Induction Machines. *IEEE Trans. Ind. Appl.* **2009**, *46*, 213–221. [CrossRef]
5. Tallam, R.; Habetler, T.; Harley, R.G. Transient model for induction machines with stator winding turn faults. *IEEE Trans. Ind. Appl.* **2002**, *38*, 632–637. [CrossRef]
6. Lee, S.B.; Tallam, R.M.; Habetler, T.G. A robust, on-line turn-fault detection technique for induction machines based on monitoring the sequence component impedance matrix. *IEEE Trans. Power Electron.* **2003**, *18*, 865–872. [CrossRef]
7. Bouzid, M.B.K.; Champenois, G. New Expressions of Symmetrical Components of the Induction Motor under Stator Faults. *IEEE Trans. Ind. Electron.* **2012**, *60*, 4093–4102. [CrossRef]
8. Seshadrinath, J.; Singh, B.; Panigrahi, B. Incipient Turn Fault Detection and Condition Monitoring of Induction Machine Using Analytical Wavelet Transform. *IEEE Trans. Ind. Appl.* **2013**, *50*, 2235–2242. [CrossRef]
9. Stafford, M.R.; Jackson, H.; Mayo-Wilson, E.; Morrison, A.P.; Kendall, T. Early interventions to prevent psychosis: Systematic review and meta-analysis. *IEEE Ind. Appl. Mag.* **2013**, *346*, 34–40. [CrossRef] [PubMed]
10. Stone, G.; Boulter, E.; Culbert, I.; Dhirani, H. Electrical insulation for rotating machines-design, evaluation, aging, testing, and repair—Book Review. *IEEE Electr. Insul. Mag.* **2004**, *20*, 65. [CrossRef]
11. Oliver, J.; Woodson, H.; Johnson, J. A Turn Insulation Test for Stator Coils. *IEEE Trans. Power Appar. Syst.* **1968**, 669–678. [CrossRef]
12. Grubic, S.; Restrepo, J.; Aller, J.; Lu, B.; Habetler, T.G. A New Concept for Online Surge Testing for the Detection of Winding Insulation Deterioration in Low-Voltage Induction Machines. *IEEE Trans. Ind. Appl.* **2011**, *47*, 2051–2058. [CrossRef]
13. Poli, R.; Kennedy, J.; Blackwell, T. Particle Swarm Optimisation. *SSRN Electron. J.* **2007**, *IV*, 1942–1948. [CrossRef]
14. Gaing, Z.-L. A Particle Swarm Optimization Approach for Optimum Design of PID Controller in AVR System. *IEEE Trans. Energy Convers.* **2004**, *19*, 384–391. [CrossRef]
15. Chang, H.-H.; Lin, L.-S.; Chen, N.; Lee, W.-J. Particle-Swarm-Optimization-Based Nonintrusive Demand Monitoring and Load Identification in Smart Meters. *IEEE Trans. Ind. Appl.* **2013**, *49*, 2229–2236. [CrossRef]
16. Yeh, Y.-C.; Tsai, M.-S. Application of PSO for the development and simulation of EV charging time minimization in distribution systems. In Proceedings of the 2015 18th International Conference on Intelligent System Application to Power Systems (ISAP), Porto, Portugal, 11–16 September 2015.
17. Santos, P.; Macedo, M.; Figueiredo, E.; Santana, C.J.; Soares, F.; Siqueira, H.; Maciel, A.; Gokhale, A.; Bastos-Filho, C.J.A. Application of PSO-based clustering algorithms on educational databases. In Proceedings of the 2017 IEEE Latin American Conference on Computational Intelligence (LA-CCI), Arequipa, Peru, 8–10 November 2017.
18. Vapnik, V.N. *Statistical Learning Theory*; John Wiley & Sons: New York, NY, USA, 1998.
19. Seshadrinath, J.; Singh, B.; Panigrahi, B.K. Single-Turn Fault Detection in Induction Machine Using Complex-Wavelet-Based Method. *IEEE Trans. Ind. Appl.* **2012**, *48*, 1846–1854. [CrossRef]

20.　Shi, J.; Lee, W.-J.; Liu, Y.; Yang, Y.; Wang, P. Forecasting Power Output of Photovoltaic Systems Based on Weather Classification and Support Vector Machines. *IEEE Trans. Ind. Appl.* **2012**, *48*, 1064–1069. [CrossRef]

21.　Pandarakone, S.E.; Mizuno, Y.; Nakamura, H. Evaluating the Progression and Orientation of Scratches on Outer-Raceway Bearing Using a Pattern Recognition Method. *IEEE Trans. Ind. Electron.* **2018**, *66*, 1307–1314. [CrossRef]